Energy Conversion and Management 228 (2021) 113665

Contents lists available at ScienceDirect

Energy Conversion and Management

journal homepage: www.elsevier.com/locate/enconman

Solar energy powered high-recovery reverse osmosis for synchronous seawater desalination and energy storage

Xiaotian Lai, Rui Long *, Zhichun Liu, Wei Liu *

School of Energy and Power Engineering, Huazhong University of Science and Technology, 1037 Luoyu Road, Wuhan 430074, China

ARTICLE INFO

Keywords:
Dish Solar Stirling Engine
Reverse Osmosis
Energy Storage
Seawater Desalination

ABSTRACT

Solar energy is clean and sustainable to power our continuously developing society, but the intermittency and unpredictability lays a barrier on its direct connection to the grid. Seawater desalination is an effective path to consume dynamic solar energy to produce fresh water and stable salinity gradient energy simultaneously. Thus, a self-diluted 2-stage reverse osmosis with high recovery ratio is proposed to consume the renewable power from a dish solar Stirling engine to achieve more water production and energy storage. Based on theoretical derivation, system performance is evaluated under ideal membrane property and enough membrane area condition. The influence of hydraulic pressure difference and diluted fraction ratio on water production and energy storage performance are investigated. A performance optimization is further conducted and the corresponding performance are evaluated. Results revealed that self-diluted 2-stage configuration can improve the maximal recovery ratio from 25%, 57% and 70% to 39%, 62% and 72% under the maximal bearable pressure difference of 4, 7 and 10 MPa. Maximal salinity gradient energy of 3.84 MJ can be stored with an overall energy efficiency of 8.42% while desalinating 1 cubic meter seawater of 0.6 M. Theoretical analysis indicates that novel configuration is potentially an effective method to improve the upper separation limitation, which further produces more water and stores more solar energy in the desalination process of finite amount of source seawater.

1. Introduction

Fresh water production and clean energy generation are both cornerstones to guarantee the continuous and stable development of human society [1]. Seawater, which covers around 70% of the earth, is regarded as one of the most potential sources for fresh water production with several developed desalination technologies [2], such as MSF (multi-stage flash) [3], MED (multi-effect distillation) [4], MD (membrane distillation) [5] and RO (reverse osmosis) [6] et al. Among the common processes, RO has flexible capacity, which achieves its successful applications from a small unit for purified water production in household [7] to a large desalination plant for megaton water production in a city [8]. Meanwhile, RO has lower SEC (specific energy consumption) as compared with other technologies, which makes it competitive in the routine operation and widely utilized for seawater desalination. However, the increasing world population also drives the rapid increase of water demand, which means further reducing SEC [9] or improving total energy supplement [10] are both effective paths to solve this huge challenge.

The theoretical lowest SEC of SWRO (seawater reverse osmosis) process is reported as 1.07 kWh/m^3 under the recovery ratio of 50%, while the current realistic value ranges between 2.5 and 4.0 kWh/m^3 [11]. As further considering the pre-treatment and post-treatment processes, the SEC of a SWRO plant is up to around 3.5–4.5 kWh/m^3 [12]. In order to cut down the SEC, different methods can be adopted before, in and after the RO process. Reducing salinity of source seawater before membrane module is capable to cut down the permeation resistance, then less pump power is required to achieve lower SEC. Certainly, energy in other forms are consumed as price, such as the natural salinity gradient energy in FO-SWRO (forward osmosis powered SWRO) system [13] or cold energy in Freezing-SWRO system [14]. In RO process, improving water permeation coefficient of membrane [15] or reducing concentration polarization [16] can enhance water permeation, thus reduces SEC. As to the discharged brine solution of RO process, increasing water production via further desalination and reducing energy consumption via energy recovery are both effective as well. Further desalination can be powered by low-grade heat to produce additional fresh water in SWRO-MD system [17]. In comparison, harvesting the residual pressure energy via high-efficiency ERD (energy recovery device) [18] or the salinity gradient energy via PRO (pressure retarded osmosis) [19] and RED (reverse electrodialysis) [20] reduces the total

* Corresponding authors.
E-mail addresses: r_long@hust.edu.cn (R. Long), w_liu@hust.edu.cn (W. Liu).

https://doi.org/10.1016/j.enconman.2020.113665
Received 3 August 2020; Received in revised form 22 October 2020; Accepted 12 November 2020
Available online 20 November 2020

Nomenclature

x	Diluted Fraction Ratio
k	Mass Transfer Coefficient, m/s
A	Water Permeation Coefficient, m/(s Pa)
A^*_m	Normalized Membrane Area
B	Salt Permeation Coefficient, m/s
C	Concentration, M
E	Energy, MJ
J_s	Transmembrane Salt Flux, mol/(m^2 s)
J_w	Transmembrane Water Flux, m/s
K	Solute Resistivity, s/m
P	Power, kW
R	Gas Constant, J/(mol K)
T	Temperature, K
V	Volume, m^3
W	Water/Width of Membrane (in Appendix A)
Y	Recovery Ratio, %
ΔG	Gibbs Free Energy, MJ
ΔP	Hydraulic Pressure Difference, MPa

Greek Symbol

η	Energy Conversion Efficiency, %
$\Delta\pi$	Osmotic Pressure Difference, MPa

Subscripts

0	Source Seawater
1	First Stage
2	Second Stage
e	Exploitable
b	Bulk Flow
in	Inlet
lim	Limitation
m	Membrane
max	Maximal Value
opti	Optimal Value
out	Outlet
B	Boundary Value/Brackish Water
C	Concentrated Solution
D	Diluted Solution
E	Electricity
F	Fresh Water
H	High Concentration
L	Low Concentration
P	Transmembrane Water Permeation
S	Seawater/Solar
T	Mixing Solution

Abbreviations

CP	Concentration Polarization
DSSE	Dish Solar Stirling Engine
ERD	Energy Recovery Device
FO	Forward Osmosis
GA	Genetic Algorithm
GT	Gas Turbine
MD	Membrane Distillation
MED	Multi-Effect Distillation
MSF	Multi-Stage Flash
ORC	Organic Rankine Cycle
PRO	Pressure Retarded Osmosis
RED	Reverse Electrodialysis
RO	Reverse Osmosis
RSP	Reverse Salt Permeation
SEC	Specific Energy Consumption, kWh/m^3
SOFC	Solid Oxide Fuel Cell
SWRO	Seawater Reverse Osmosis

energy input.

With the development of energy saving technologies, the realistic SEC will gradually approach the lower limit. Thus, improving energy supplement for desalination will provide a wider solution path for water scarcity. Compared with fossil fuel, clean and renewable energy sources such as hydrogen fuel, salinity gradient, wind, tidal and solar energy are more competitive for they have no harmful emission [21]. Valerie Eveloy et al. integrated a SWRO unit driven by ORC (organic Rankine cycle) to the bottom of SOFC-GT (solid oxide fuel cell–gas turbine) system, hydrogen energy is consumed as fuel to cogenerate clean electricity and water [22]. Wei He et al. utilized the concentrated seawater from reverse osmosis process to pair with brackish water and release the salinity gradient energy to power a stand-alone SWRO [23]. Baltasar Peñate et al. adopted wind energy to drive a SWRO system and compared the system performance under gradual and fixed capacity. Results indicate that gradual capacity is recommended for the SWRO system driven by wind [24]. Agustín M. Delgado-Torres et al. adopted tidal energy to assist a solar powered SWRO system, which is capable to increase the annual operating time from 19.6% to 41.7% of a year [25]. In the clean energy sources stated above, solar energy is widely distributed and can be converted into electricity via multi methods such as photovoltaic panel [26], thermophotovoltaic cell [27] or solar thermal power cycles [28], which expands its opportunity to power SWRO [29]. Hamid Reza Abbasi et al. [30] utilized phase change material to store the thermal energy in a solar tower and drive thermodynamic cycle to power SWRO, and Harsh Vyas et al. [31] utilized photovoltaic panel to power SWRO. Among the common solar power technologies, DSSE (dish solar Stirling engine) operates with high solar-electricity energy efficiency and flexible power capacity [32]. Integrating DSSE and SWRO is capable to produce water in a community for distributed application or a large farm for centralized application.

In addition, energy storage accompanies with water production in a desalination process as well [33]. Thus, the hybridization of DSSE and SWRO is also a potential solution to push the further exploitation of solar and salt gradient energy utilization. Influenced by the drastic variation of solar illumination intensity in a day, power output of a solar energy system always fluctuates with time [34]. The uncertainty of power output in the next minute limits the effective match of energy supplement and demand. Commonly, energy storage system such as upstream thermal storage module [35] or downstream battery module [36] is always installed in the solar power system to stabilize the power output. In comparison, salinity gradient energy is more stable, but the finite intensity of natural concentration difference only generates finite power density which limits the application of natural salinity gradient energy [37]. In DSSE-SWRO hybrid system, the dynamic solar power is consumed to desalinate the seawater and stabilized as additional salinity gradient energy in the brine solution, which also enhances the natural salinity gradient simultaneously. Thus, stable and clean power can be generated from the solar and salinity gradient energy. Furthermore, the more water is extracted from seawater, the more dynamic solar power is stored as additional salinity gradient energy based on the natural salinity gradient energy in the brine solution, which will consequently improve the downstream energy releasing performance [38]. Hence, the SWRO module should operate with high-recovery in the DSSE-SWRO system. Extending the membrane area to fully utilize the hydraulic pressure difference or elevating the operating pressure of RO module

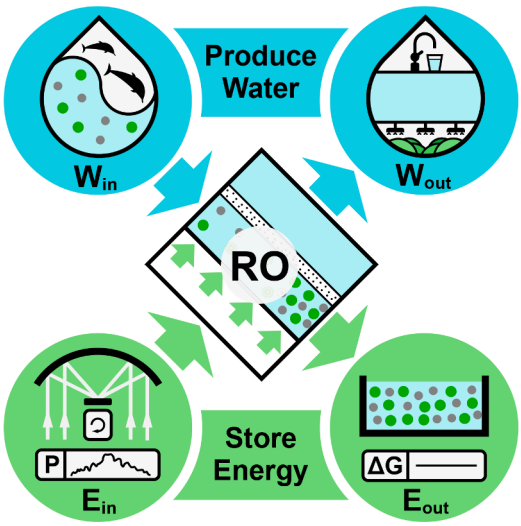

Fig. 1. Dish solar Stirling engine powered seawater reverse osmosis system.

can increase the recovery ratio. However, the thin film semi-permeable membrane has a maximal bearable pressure limitation which prevents its damage. Toray Industries ever developed a RO membrane which can endure the high pressure of 8–10 MPa [39]. The high pressure membrane technology allows the further desalination of RO brine solution from the previous stage, which improves the recovery ratio from 40% to 60% [40].

In order to further improve the recovery ratio of SWRO module to achieve better water production and energy storage performance under workable pressure difference. Osmotic pressure in the diluted channel is utilized to improve the outlet concentration of concentrated solution under maximal bearable pressure difference in a novel self-diluted 2-stage SWRO. Previous work such as osmotically assisted reverse osmosis system proposed by Timothy V. Bartholomew et al. [41], cascading osmotically mediated reverse osmosis system proposed by Xi Chen et al. [42] and split-feed counterflow reverse osmosis system proposed by Andrew T. Bouma et al [43] all demonstrate the theoretical availability of the utilization of osmotic pressure in the diluted channel. In this work, partial source seawater is fed as barometric diluted solution and the rest is fed as pressurized concentrated solution in cocurrent flow to produce diluted and concentrated seawater at the first stage. Then, the diluted seawater is desalinated at the second stage to produce more fresh water with lower inlet concentration under the maximal bearable pressure condition. The influence of hydraulic pressure difference and diluted fraction ratio on the water production and energy storage performance are investigated. A performance optimization is further conducted and the corresponding water production and energy storage performance are evaluated with the derived analytical solution. This study offers an alternative efficient way for solar energy powered seawater desalination and energy storage with better theoretical performance.

2. Methods and quantification

As depicted in Fig. 1, green solar power generated from DSSE is utilized to power a high-recovery RO unit to desalinate the pretreated seawater. Under higher recovery ratio, the fed seawater can be separated into fresh solution with more quantity and brine solution with higher concentration. Thus, more fresh water is produced for drinking or irrigation, and more dynamic solar power is stored as stable salinity gradient. Besides, the harmful emission in the energy and matter conversion procedures are both zero.

In RO process, the applied pressure on feed solution overcomes the osmotic resistance then drives the fresh water permeation. Meanwhile, the osmotic resistance will increase continuously with the concentration of feed solution until it equals to the applied pressure difference and ends the water permeation as depicted in Fig. 2(a). Thus, increasing hydraulic pressure difference is a method to discharge brine solution with higher concentration, which means more fresh water production and energy storage can be achieved. Thus, as the hydraulic pressure

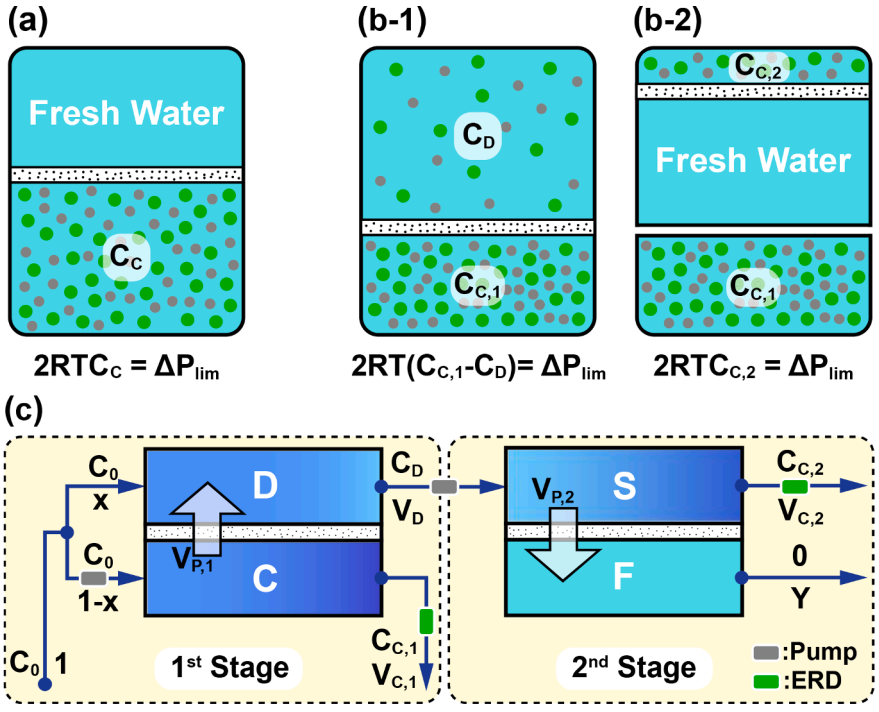

Fig. 2. Seawater reverse osmosis under the maximal bearable pressure difference: (a) Seawater as feed solution and fresh water as permeate solution; (b) Partial seawater as feed solution and partial seawater as permeate solution for self-dilution at the first stage (b-1), diluted seawater as feed solution and fresh water as permeate solution for water production at the second stage (b-2); (c) Continuous self-diluted 2-stage seawater reverse osmosis configuration.

difference approaches ΔP_{lim} (maximal bearable pressure difference of membrane), recovery ratio of the seawater-water paired RO configuration in Fig. 2(a) reaches its upper limitation.

To further improve the recovery ratio under ΔP_{lim}, the 2-stage RO configuration depicted in Fig. 2(b) can be adopted. In Fig. 2(b-1) and (c), certain fractions of seawater are utilized as concentrated and diluted solutions respectively at the first stage. For the diluted seawater has a concentration over zero, the concentration of discharged brine solution at the first stage can be higher than Fig. 2(a) under the same pressure. Then, the diluted seawater is utilized as feed solution for water extraction and discharged at the second stage in Fig. 2(c) with the same concentration in Fig. 2(a). As the concentration of total brine discharge in Fig. 2(b) is higher than Fig. 2(a), recovery ratio can be enhanced.

- Slight reverse salt permeation is neglected;
- Slight variation of seawater volume with concentration is neglected;
- Membrane area is enough to achieve complete fresh water permeation.

With the first assumption, the molar conservation of dissolved ions in concentrated and diluted channels have Eqs. (1) and (2). As 1 m^3 source seawater enters the inlet, Eq. (3) is established by the second assumption. According to the third assumption, transmembrane water flux will end at the outlet under enough membrane area, which means the local concentration polarization is extremely slight. Thus, the bulk concentration can be utilized to evaluate the osmotic pressure difference which equals to the hydraulic pressure difference. In Eqs. (1)–(4), x represents the diluted fraction ratio.

$$C_0(1-x) = C_{C,1}V_{C,1} \tag{1}$$

$$C_0 x = C_D V_D \tag{2}$$

$$V_{C,1} + V_D = 1 \tag{3}$$

$$2RT(C_{C,1} - C_D) = \Delta P \tag{4}$$

With the derivation in Appendix A.1, the volume and concentration of the brine discharge at the first stage have Eqs. (5) and (6).

$$V_{C,1} = \left(\frac{RTC_0}{\Delta P} + \frac{1}{2}\right) - \sqrt{\frac{RTC_0}{\Delta P}(2x-1) + \left(\frac{RTC_0}{\Delta P}\right)^2 + \left(\frac{1}{2}\right)^2} \tag{5}$$

$$C_{C,1} = \frac{C_0(1-x)}{V_{C,1}} = \frac{C_0(1-x)}{\left(\frac{RTC_0}{\Delta P} + \frac{1}{2}\right) - \sqrt{\frac{RTC_0}{\Delta P}(2x-1) + \left(\frac{RTC_0}{\Delta P}\right)^2 + \left(\frac{1}{2}\right)^2}} \tag{6}$$

The volume and concentration of the discharged solution at the second stage can be derived as Eqs. (7) and (8) according to the conservation of dissolved ions in diluted solution and the outlet pressure relationship as well.

$$V_{C,2} = \frac{C_0 x}{C_{C,2}} = 2\frac{RTC_0}{\Delta P}x \tag{7}$$

$$C_{C,2} = \frac{\Delta P}{2RT} \tag{8}$$

Thus, the overall recovery ratio has Eq. (9).

$$\begin{aligned} Y &= 1 - V_{C,1} - V_{C,2} \\ &= \sqrt{\frac{RTC_0}{\Delta P}(2x-1) + \left(\frac{RTC_0}{\Delta P}\right)^2 + \left(\frac{1}{2}\right)^2} - 2\frac{RTC_0}{\Delta P}x - \frac{RTC_0}{\Delta P} + \frac{1}{2} \end{aligned} \tag{9}$$

SEC is derived according to Eq. (10), in which the pressurization of source seawater $(1-x)$ at the first stage and diluted seawater $(x + V_{P,1})$ at the second stage consumes pump work, and ERD harvests residual pressure of discharged solution. The further expansion of SEC in Eq. (10) reveals its precise components those are the energy consumed for pressurizing the transmembrane water permeation from the first stage, energy consumed for pressurizing the total source seawater and energy recovered by ERD for producing 1 m^3 fresh water. By substituting the formulations of $V_{P,1}$ and Y into Eq. (10), SEC can be described as Eq. (11).

$$\begin{aligned} \mathrm{SEC} &= \frac{\Delta P\left[(1-x) + (x + V_{P,1})\right] - \Delta P(1-Y)\eta_{ERD}}{Y} \\ &= \Delta P\frac{V_{P,1}}{Y} + \Delta P\frac{1}{Y} - \Delta P\frac{(1-Y)}{Y}\eta_{ERD} \end{aligned} \tag{10}$$

$$\mathrm{SEC} = \left[\frac{\sqrt{\frac{RTC_0}{\Delta P}(2x-1) + \left(\frac{RTC_0}{\Delta P}\right)^2 + \left(\frac{1}{2}\right)^2} - x - \frac{RTC_0}{\Delta P} + \frac{3}{2} - \eta_{ERD}}{\sqrt{\frac{RTC_0}{\Delta P}(2x-1) + \left(\frac{RTC_0}{\Delta P}\right)^2 + \left(\frac{1}{2}\right)^2} - 2\frac{RTC_0}{\Delta P}x - \frac{RTC_0}{\Delta P} + \frac{1}{2}} + \eta_{ERD}\right]\Delta P \tag{11}$$

Eqs. (9) and (11) indicate that recovery ratio and SEC are both closely related to the diluted fraction ratio (x). As x equals to 0 or 1, it means that the real separation process only occurs at one of the two stages (the first or second stage). Thus, recovery ratio can be simplified as Eq. (12) which is exactly equal to that of conventional seawater-water paired SWRO in Fig. 2(a).

$$Y_B = 1 - 2\frac{RTC_0}{\Delta P}(x = 0 \text{ or } 1) \tag{12}$$

As to the SEC when x equals to 1, all the seawater passes through the diluted channel with no energy consumption or harvesting at the first stage, and the separation process only occurs at the second stage. Hence, the corresponding SEC in Eq. (13) is equal to that of Fig. 2(a).

$$\mathrm{SEC}_B = \frac{\Delta P - \eta_{ERD}(1-Y_B)\Delta P}{Y_B}(x = 1) \tag{13}$$

In comparison, the separation process as $x = 0$ only occurs at the first stage. However, the transmembrane water permeation from the first stage is pressurized again at the inlet of the second stage for water production though no salt needs to be filtered at the second stage. Thus, the corresponding SEC in Eq. (14) is higher than Eq. (13).

$$SEC_B = \frac{\Delta P - \eta_{ERD}(1-Y_B)\Delta P + Y_B\Delta P}{Y_B}(x = 0) \tag{14}$$

Salinity gradient energy exists between the solutions with concentration difference and can be quantified by Gibbs free energy in Eq. (15) [44]. With the separation in RO unit, Gibbs free energy appears with the concentration difference from zero. Thus, the Gibbs free energy stored between the concentrated and fresh solutions in the desalination process of 1 m^3 seawater has Eq. (16) with the derivation in Appendix A.2. Eqs. (17) and (18) are the energy conversion efficiency of SWRO process and the whole system.

$$\Delta G = 2RT(V_H C_H ln\frac{C_H}{C_T} + V_L C_L ln\frac{C_L}{C_T}) \tag{15}$$

$$\Delta G_{RO} = 2RTC_0 ln\frac{1}{1-Y} \tag{16}$$

$$\eta_{RO} = \frac{\Delta G_{RO}}{\Delta P(1+V_{P,1}) - \Delta P(1-Y)\eta_{ERD}} \tag{17}$$

$$\eta = \eta_{DSSE}\eta_{RO} \tag{18}$$

Eq. (16) indicates that more Gibbs free energy can be stored with the increase of recovery ratio. However, considering the produced fresh water has high level for drinking, the concentrated solution should be coupled with other low-concentration solutions such as fresh river (F), brackish (B) or even seawater (S) to release salinity gradient power. The exploitable Gibbs free energy in the mixing process of 0.5 m^3 concentrated solution and 0.5 m^3 low-concentration solution has Eq. (19).

$$\Delta G_e = RT(C_C ln\frac{2C_C}{C_C + C_L} + C_L ln\frac{2C_L}{C_C + C_L}) \tag{19}$$

Table 1
Initial values for case study.

Water salinities	C_0/C_S (M)	C_B (M)	C_F (M)
	0.6	0.3	0.005
Operational parameters	x (–)	ΔP (MPa)	T (K)
	0.5	7	298.15

3. Results and discussion

In order to investigate the performance systematically, case study, sensitivity analysis and performance optimization are conducted sequentially based on the derived equations stated above. Water production and energy storage performance of conventional 1-stage reverse osmosis is set as comparison benchmark, the theoretical performance of novel configuration is evaluated and analyzed precisely.

3.1. Case study

To start with, water production and energy storage performance of the proposed system are evaluated and compared with conventional 1-stage seawater-water paired configuration.

With the initial values listed in Table 1, 1 m^3 seawater with the concentration of 0.6 M is selected as total feed solution. At the first stage, half of the seawater flows through diluted channel to extract water from the other half in concentrated channel under the hydraulic pressure difference of 7 MPa. Then, diluted seawater is fed into the second stage for fresh water production under the same pressure difference.

As shown in Fig. 3(a), the recovery ratio is enhanced from 57.51% to 61.83%, which means more fresh water of 43 L can be produced from 1 m^3 seawater by the 2-stage configuration under the maximal bearable pressure difference of 7 MPa. Fig. 3(b) reveals the mechanism of recovery ratio enhancement. Area I + II encircled by black solid line and II + III encircled by red solid line both represent the total molar of NaCl

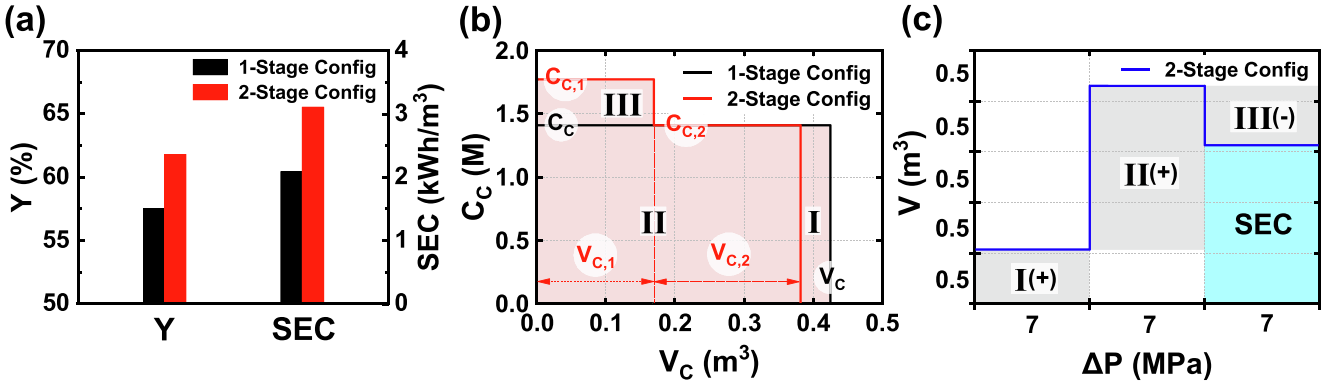

Fig. 3. Comparison of water production performance and discharged brine solution property between 2-stage and 1-stage configurations in (a) and (b), components of specific energy consumption of 2-stage configuration in (c).

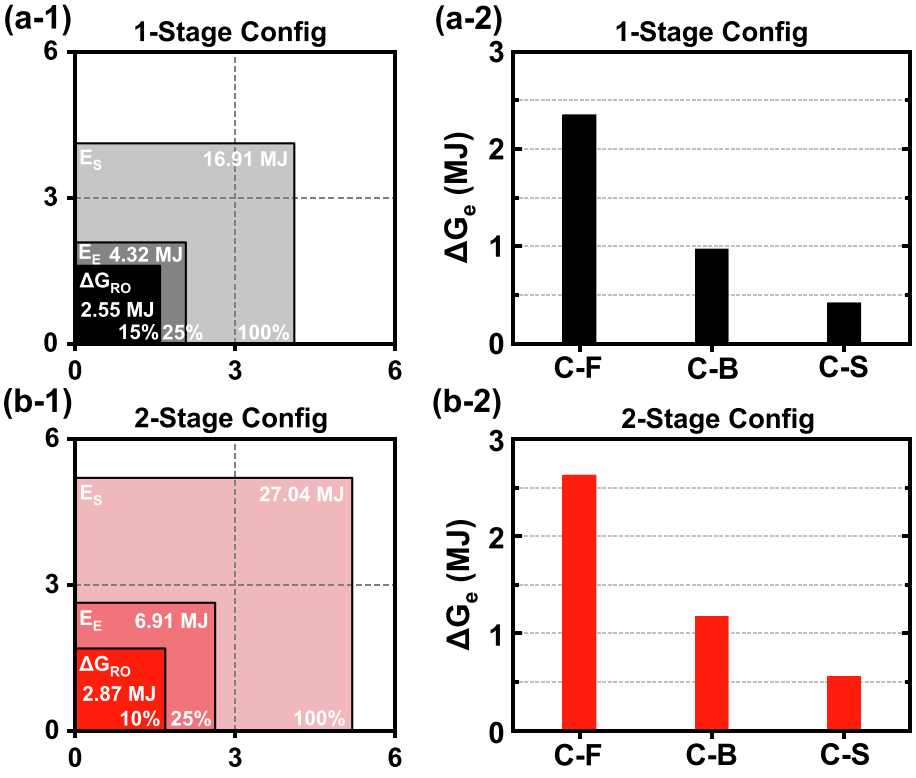

Fig. 4. Comparison of energy storage performance between 2-stage and 1-stage configurations.

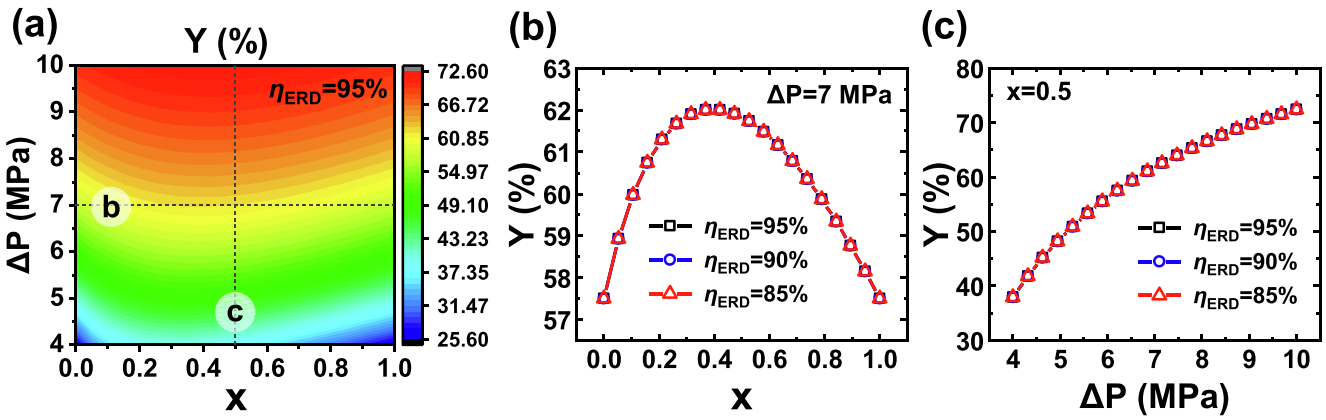

Fig. 5. Influence of diluted fraction ratio and hydraulic pressure difference on recovery ratio under different efficiency of energy recovery device.

(sodium chloride) dissolved in the source seawater. It can be seen that 1 m^3 seawater is concentrated to 0.42 m^3 brine solution with the concentration of 1.41 M by the 1-stage configuration. Higher discharge concentration of 1.77 M at the first stage in 2-stage configuration further accommodates the NaCl from area I to area III, thus to improve the recovery ratio. Certainly, more energy is required to produce fresh water with higher recovery ratio. Fig. 3(a) indicates that SEC increases significantly from 2.09 to 3.10 kWh/m^3. The grey area I(+) and II(+) in Fig. 3(c) represent the pump work consumed for pressurizing the transmembrane water permeation from the first stage and the total 1 m^3 source seawater, while III(−) represents the harvested energy by ERD. Compared with 1-stage configuration, the pressurization of transmembrane water permeation from the first stage at the inlet of the second stage requires additional energy of area I(+), which induces the increase of SEC (blue area).

Fig. 4(a-1) depicts the energy storage performance while desalinating 1 m^3 seawater by DSSE powered 1-stage SWRO. With an electric energy input of 4.32 MJ, Gibbs free energy of 2.55 MJ is produced between the fresh and concentrated solutions with an efficiency of 59%. Considering DSSE has a solar-electricity conversion efficiency of 25.56% [45], the consumed solar energy is 16.91 MJ and the overall efficiency is 15%. Paring 0.5 m^3 concentrated solution with 0.5 m^3 of fresh river water, brackish estuarial water or saline seawater, corresponding Gibbs free energy in Fig. 4(a-2) is 2.35, 0.97 and 0.41 MJ respectively. Fig. 4(b-1) depicts the energy storage performance of DSSE powered 2-stage SWRO. With the increase of concentration, stored Gibbs free energy in the desalination process of 1 m^3 seawater is enhanced to 2.87 MJ. And the exploitable Gibbs free energy for different solution pairs is increased

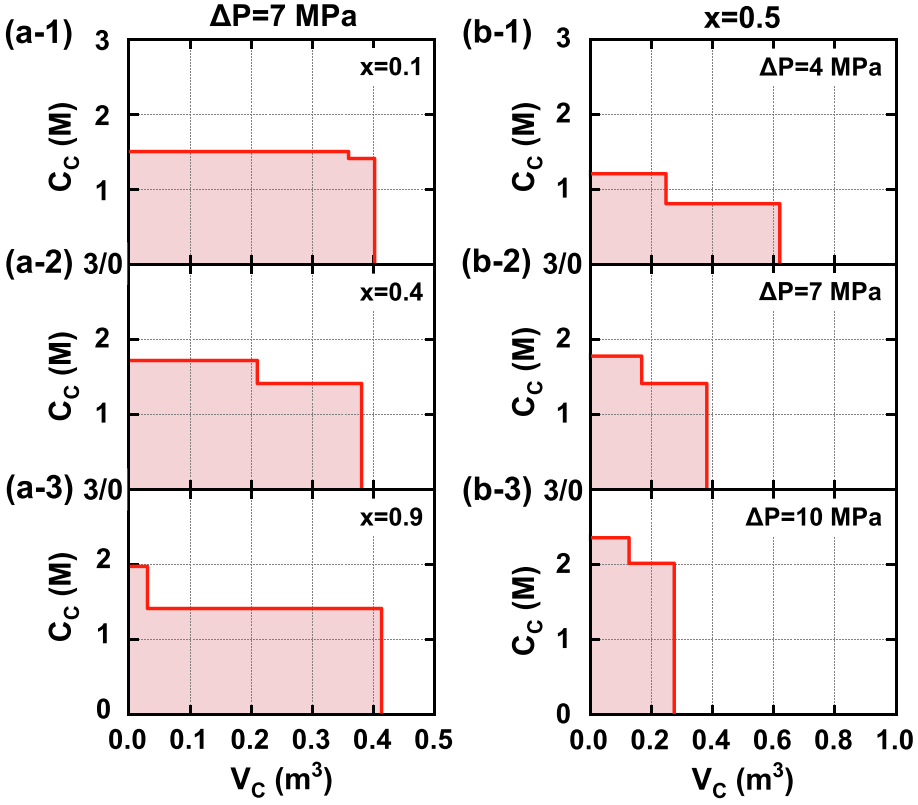

Fig. 6. Comparison of discharged brine solution under different diluted fraction ratio in (a) and hydraulic pressure difference in (b).

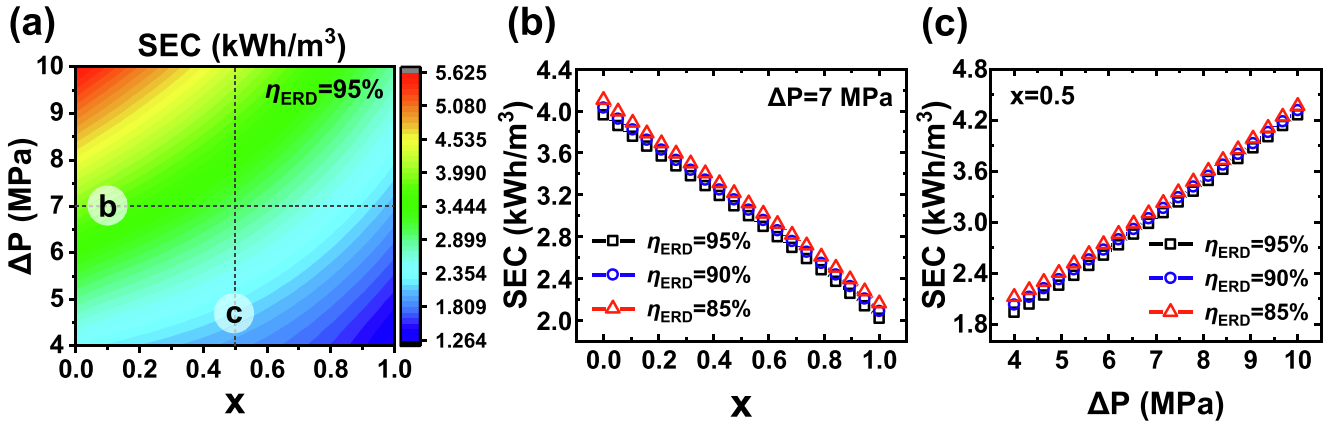

Fig. 7. Influence of diluted fraction ratio and hydraulic pressure difference on specific energy consumption under different efficiency of energy recovery device.

to 2.62, 1.17 and 0.55 MJ respectively in Fig. 4(b-2). However, 2-stage configuration has lower RO efficiency of 41%, which increases the renewable electrical and solar energy consumption to 6.91 and 27.04 MJ while the overall efficiency is reduced to 10%.

With the results of case study, it can be seen that 2-stage configuration is capable to enhance the water production ability significantly while the increase of SEC is drastic as well. In addition, the 2-stage configuration is also capable to convert more fluctuating solar energy into stable salinity gradient energy with higher concentration difference, which can improve the amount of stabilized energy and enhance the energy releasing intensity of salinity gradient power system simultaneously.

3.2. Sensitivity analysis

The derived equations indicate that the separation performance is closely related to the operational parameters (diluted fraction ratio and hydraulic pressure difference). Thus, the influence of operational parameters on water production and energy storage performance of DSSE powered 2-stage SWRO system is investigated and analyzed in this part. The diluted fraction ratio varies from 0 to 1 and hydraulic pressure difference varies from 4 to 10 MPa.

Fig. 5 shows the influence of diluted fraction ratio and hydraulic pressure difference on recovery ratio under different efficiency of ERD. In Fig. 5(a), the increase of diluted fraction ratio from 0 to 1 and

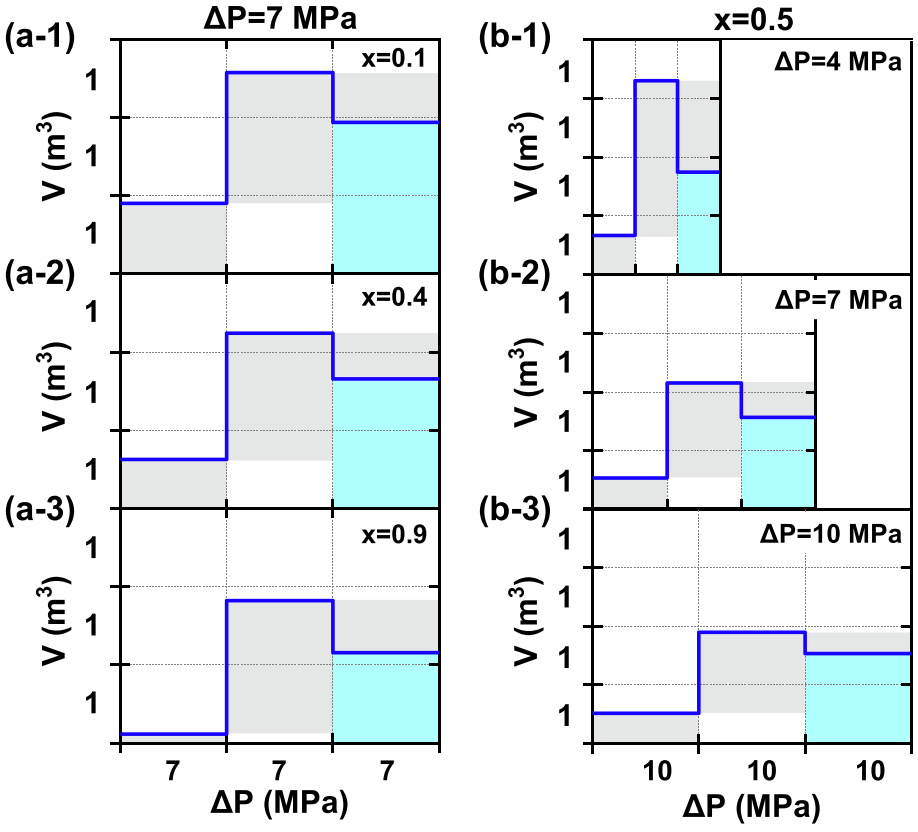

Fig. 8. Comparison of specific energy consumption components under different diluted fraction ratio in (a) and hydraulic pressure difference in (b).

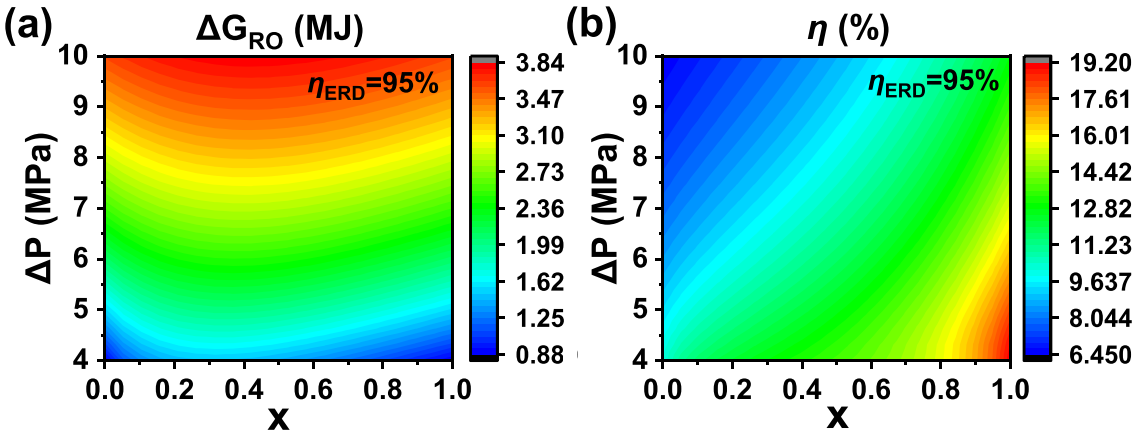

Fig. 9. Influence of diluted fraction ratio and hydraulic pressure difference on energy storage performance.

hydraulic pressure difference from 4 to 10 MPa induces great variation of recovery ratio from 25% to 72%. Comparing the results horizontally under pressure difference of 7 MPa in Fig. 5(b), it can be seen that recovery ratio appears the trend of increasing before decreasing and is not affected by the energy efficiency of ERD. Namely, the 2-stage SWRO under an arbitrary x ($0 < x < 1$) is capable to produce more water than 1-stage configuration and optimal diluted fraction ratio exists to achieve the maximal recovery ratio. According to the properties of discharged solutions under different diluted fraction ratio ($x = 0.1$, 0.4 and 0.9) in Fig. 6(a), it can be seen that the discharged solution at the first stage as x equals to 0.1 has high volume but low concentration improvement and the discharged solution at the first stage as x equals to 0.9 has high concentration improvement but low volume, which are both not capable to enrich more salt into the discharged solution at the first stage. In comparison, a moderate diluted fraction ratio of 0.4 is capable to extract more water from the concentrated solution at the first stage, for more salt can be enriched to the discharged solution with appropriate concentration improvement and solution volume.

The vertical comparison of recovery ratio in Fig. 5(c) indicates that higher hydraulic pressure difference is beneficial for improving recovery ratio significantly. Under the diluted fraction ratio of 0.5, recovery ratio increases from 38% to 72%. As the driving force of reverse osmosis, greater hydraulic pressure difference will end the water permeation with greater outlet osmotic pressure difference. Thus, the concentration of discharged solutions from the first and second stages are both improved with the increase of hydraulic pressure difference in Fig. 6(b). Namely, the total dissolved NaCl (area in pink) is enriched into less volume of concentrated solution which is depicted on the X axial. Hence, high recovery is achieved with more fresh water extraction from the inlet source seawater.

As to the SEC of 2-stage configuration, the results depicted in Fig. 7 (a) indicate that SEC varies from 1.26 kWh/m^3 to 5.62 kWh/m^3 with the variance of diluted fraction ratio and hydraulic pressure difference under the ERD efficiency of 95%. Fig. 7(b) further indicates that the SEC under 7 MPa drops gradually with the increase of diluted fraction ratio, and the increase of ERD efficiency from 85% to 95% is capable to further reduce SEC by 0.5 kWh/m^3. According to the components of SEC in Eq. (10), the three parts of SEC under different diluted fraction ratio is depicted in Fig. 8(a). The analysis in case study indicates that the three areas in grey represent the energy consumption by pressurization of transmembrane water permeation from the first stage and the total source seawater, and energy harvested by ERD. It can be seen that, with the increase of diluted fraction ratio, energy consumption for the pressurization of the transmembrane water permeation drops significantly while the other two parts vary slightly. As treating 1 m^3 source seawater, the increase of diluted fraction ratio (x) represents less seawater is fed into the concentrated channel ($1 - x$) at the first stage. Thus, the transmembrane water permeation from the first stage drops significantly and leads to the drop of SEC (blue area). Meanwhile, the improvement of ERD efficiency is capable to increase the area of the third area in grey and reduce the SEC as well.

In comparison, the increase of hydraulic pressure difference induces the increase of SEC in Fig. 7(c). Under the ERD efficiency of 95%, SEC increases from 1.93 to 4.26 kWh/m^3. According to the components of SEC under different hydraulic pressure difference in Fig. 8(b), low pressure difference of 4 MPa provides weak driving force for water permeation so that more source seawater (height of grey area) needs to be pressurized to produce 1 m^3 fresh water in Fig. 8(b-1). With the increase of hydraulic pressure difference, less source seawater is required to produce 1 m^3 fresh water (shortening of the height of grey area II). However, higher hydraulic pressure difference means the energy consumption for 1 m^3 pressurized solution is getting stronger as well. Thus, higher hydraulic pressure difference is capable to cut down the amount of pressurized solution but the increase of energy consumption density is more significant. This will lead to the increase of SEC which is plotted by the blue area.

Fig. 9 depicts the stored Gibbs free energy and solar-Gibbs free energy conversion efficiency of DSSE powered 2-stage SWRO system. High pressure difference and moderate diluted fraction ratio are beneficial for achieving more energy storage as desalinating 1 m^3 seawater. Within the calculation range, the highest Gibbs free energy of 3.84 MJ is obtained. According to Eq. (16), the stored Gibbs free energy is positively related to recovery ratio. Higher recovery ratio means deeper separation process with more energy consumption and storage. In Fig. 9(b), the energy conversion efficiency exhibits a monotonic dependence with diluted fraction ratio and hydraulic pressure difference. The maximal energy conversion efficiency of 19.2% appears as the diluted fraction ratio is 1 and hydraulic pressure difference is 4 MPa, while the minimal efficiency is 6.5% as the diluted fraction ratio is 0 and the hydraulic pressure difference is 10 MPa. Therefore, operating the DSSE powered 2-stage SWRO system under high hydraulic pressure difference and a moderate diluted fraction ratio is capable to achieve high recovery ratio and store more dynamic solar energy as stable Gibbs free energy with stronger intensity.

3.3. Performance optimization

Sensitivity study indicates that optimal diluted fraction ratio exists to achieve the maximization of recovery ratio. Thus, optimization of diluted fraction ratio to maximize the recovery ratio under different maximal bearable pressure difference is conducted in this part. Deriving the recovery ratio (Y) with respect to diluted fraction ratio (x) according

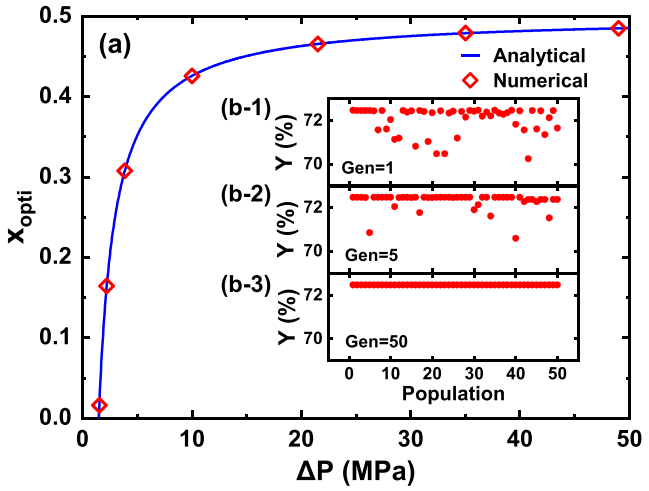

Fig. 10. Optimization of diluted fraction ratio for maximization of recovery ratio under different maximal bearable pressure difference.

to Eq. (9) and letting the derivative formula equal to zero in Eq. (20) yield to the analytical solution of optimal diluted fraction ratio in Eq. (21).

$$\frac{dY}{dx}=\frac{1}{2\sqrt{\left(\frac{RTC_0}{\Delta P}\right)^2+\left(\frac{1}{2}\right)^2+\frac{RTC_0}{\Delta P}(2x-1)}}-1=0 \tag{20}$$

$$x_{\text{opti}}=\frac{1}{2}\left(1-\frac{RTC_0}{\Delta P}\right) \tag{21}$$

In order to verify the analytical solution derived above, numerical optimization based on GA (genetic algorithm) is also conducted and the results are compared with analytical solution. Compared with analytical optimization, numerical optimization adopts different optimization path, in which the fast computing speed of computer is utilized to find the optimal value by forward search.

Fig. 10(b) depicts the process of finding the optimal diluted fraction ratio under the maximal bearable pressure difference of 10 MPa by numerical method. Recovery ratio is set as the fitness function and the arbitrarily generated populations at the first generation in Fig. 10(b-1) gradually evolves in the next generations. Most populations at the fifth generation in Fig. 10(b-2) are approaching the optimal value and all the populations finally converges at the fiftieth generation in Fig. 10(b-3). Comparing the optimal dilution ratio obtained by different methods in Fig. 10(a), the numerically optimized diluted fraction ratio under the selected sample pressure differences fit well with the analytical solution curve. Hence, the analytical optimal diluted fraction ratio derived in Eq. (21) is reliable. Further analysis of Eq. (21) indicates that lower maximal bearable pressure difference corresponds to smaller optimal diluted fraction ratio, and the optimal diluted fraction ratio gradually increases and approaches 0.5 with the increase of maximal bearable pressure difference. Dividing 1 m^3 seawater in Eq. (9) into two parts of x and $1-x$, recovery ratio in Eq. (22) can be presented as the sum of two parts in the square brackets.

$$Y=1-V_{C,1}-V_{C,2}=[(1-x)-V_{C,1}]+[x-V_{C,2}] \tag{22}$$

The first part in Eq. (22) represents the water permeation from the first stage, and the second part represents the water extracted from the desalination of x m^3 source seawater by seawater-water paired SWRO at the second stage. According to Eq. (22), smaller x_{opti} under lower maximal bearable pressure difference means that more water extraction occurs at the first stage and less water extraction occurs at the second stage. The most significant difference between the first and second stage is the inlet resistance (inlet osmotic pressure difference of RO module) for water permeation. As the driving force of water permeation in RO process, hydraulic pressure difference meets no inlet resistance at the first stage (no inlet concentration difference) while the inlet resistance is significant (significant inlet concentration difference) at the second stage. When hydraulic pressure difference is down to approach the inlet

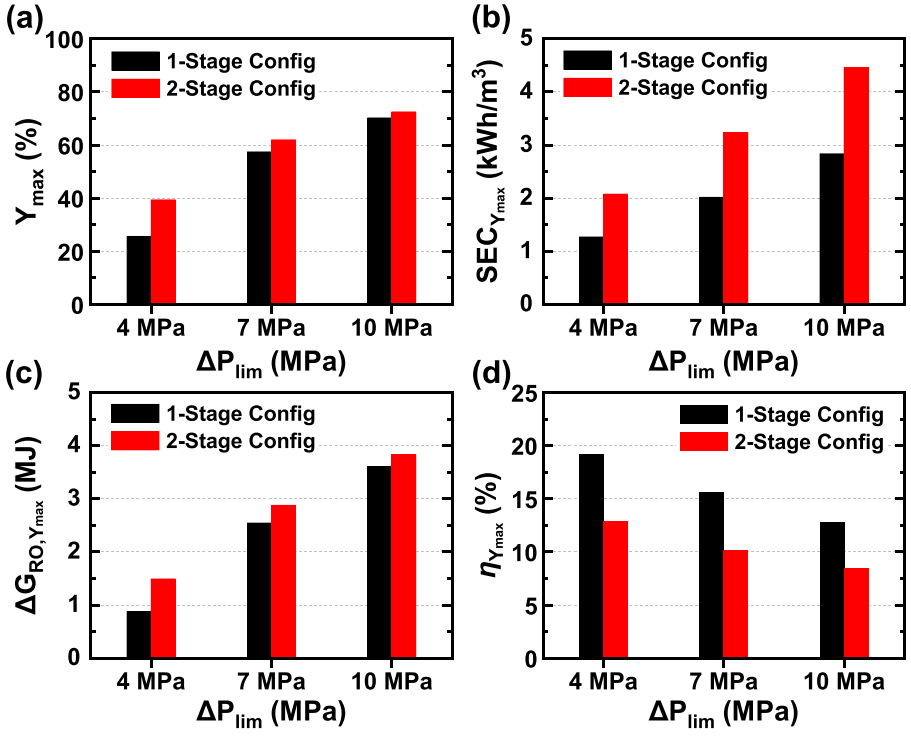

Fig. 11. Comparison of optimal water production and energy storage between 1-stage and 2-stage configurations under different maximal bearable pressure difference.

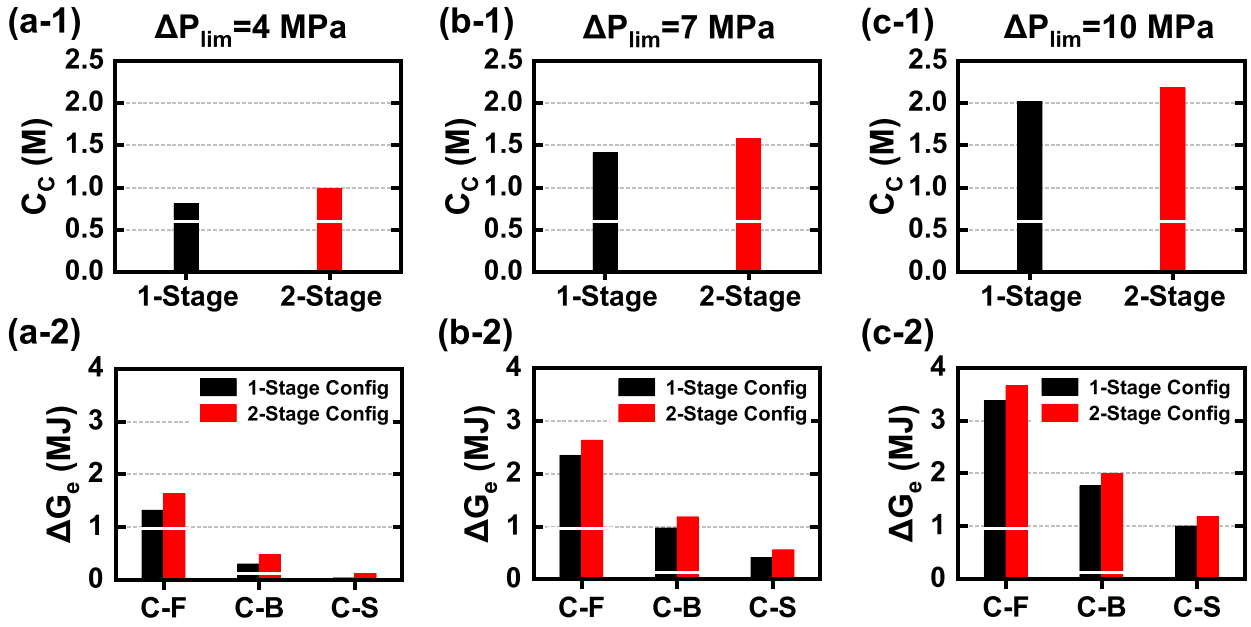

Fig. 12. Comparison of maximal exploitable Gibbs free energy of 0.5 m^3 discharged brine solution paired with 0.5 m^3 different low-concentration solution between 1-stage and 2-stage configurations under different maximal bearable pressure difference.

osmotic pressure difference at the second stage, water is hard to be driven across the membrane at this stage. Thus, more water permeation should occur at the first stage to achieve high recovery ratio, which exactly corresponds to a small diluted fraction ratio. With the continuous increase of maximal bearable pressure difference, the inlet net driving force at the two stages are getting closer, which makes the 2-stage configuration behave like the 1-stage configuration. Especially as diluted fraction ratio is closer to 0 or 1, the operation of 2-stage configuration approaches the 1-stage desalination by the first or second stage. In comparison, a diluted fraction ratio of 0.5 is the furthest condition away from the 1-stage desalination condition under high maximal bearable pressure difference. Thus, the optimal diluted fraction ratio increases with the increase of maximal bearable pressure difference and gradually approaches 0.5.

Further substituting the optimal diluted fraction ratio into Eq. (9), equation of the maximal recovery ratio of self-diluted 2-stage SWRO can be derived as Eq. (21), in which the number of maximal recovery ratio equals to the four times of the square of optimal diluted fraction ratio.

$$Y_{\max} = \left(\frac{RTC_0}{\Delta P} - 1\right)^2 = 4x_{\text{opti}}^2 \tag{23}$$

Fig. 11 depicts the comparison of maximal water production and energy storage performance between DSSE powered 1-stage and 2-stage SWRO systems while operating the systems under different maximal bearable pressure difference. The maximal bearable pressure difference of 4, 7 and 10 MPa represents the membrane which has low, middle and high mechanical intensity respectively. The water production ability in Fig. 11(a) and (b) indicate that recovery ratio can be enhanced significantly in 2-stage configuration with more energy consumption. Under the maximal bearable pressure difference of 4, 7 and 10 MPa, the maximal recovery ratio is enhanced from 25%, 57% and 70% to 39%, 62% and 72% respectively. The corresponding SEC is increased from 1.27, 2.02 and 2.84 kWh/m^3 to 2.08, 3.25 and 4.46 kWh/m^3. Results indicate that the enhancement of recovery ratio becomes smaller with the increase of the maximal bearable pressure difference. With the analysis above, the increase of maximal bearable pressure difference will make the 2-stage configuration behave like the 1-stage configuration, which consequently induces the weaker enhancement. As to the energy storage performance in Fig. 11(c) and (d), maximal Gibbs free energy of 3.84 MJ between the produced fresh and brine solutions can be generated while desalinating 1 m^3 source seawater under 10 MPa with 2-stage configuration. However, the lowest solar-Gibbs free energy efficiency of 8.42% is paid as price. In comparison, the overall efficiency under maximal bearable pressure difference of 4 MPa is 12.91% while the generated Gibbs free energy is 1.49 MJ.

Fig. 12 depicts the maximal brine concentration and corresponding exploitable Gibbs free energy as coupled with different low-concentration water source under different maximal bearable pressure difference. The white breaks in the black and red bars represent the basic concentration and exploitable Gibbs free energy of the natural seawater with concentration of 0.6 M. Higher maximal bearable pressure difference is capable to achieve more significant improvement of outlet concentration and exploitable Gibbs free energy, and 2-stage configuration can achieve further enhancement. Under the maximal bearable pressure difference of 4 MPa, the exploitable Gibbs free energy is enhanced to 1.63 MJ by 2-stage configuration as 0.5 m^3 fresh river water is paired with 0.5 m^3 brine solution which has an enhanced concentration of 0.99 M. Increasing of maximal bearable pressure difference to 10 MPa further improves the brine concentration and Gibbs free energy to 2.18 M and 3.66 MJ in 2-stage configuration, which has a relative improvement of 8% in brine concentration and Gibbs free energy as compared with 1-stage configuration.

4. Conclusion

In this study, a cocurrent self-diluted 2-stage seawater reverse osmosis configuration is proposed to improve the recovery ratio under maximal bearable pressure difference to consume seawater and dynamic solar power for synchronous water production and energy storage. With deeper enrichment of dissolved salts into the discharged solution at the first stage, higher water recovery ratio can be achieved by the 2-stage configuration, thus to guarantee better water production and energy storage performance. Theoretical analysis and optimization are conducted to evaluate the water production and energy storage performance of the 2-stage configuration under ideal membrane property and enough membrane area condition. Results indicate that decreasing

diluted fraction ratio contributes to SEC and energy efficiency. There exists an optimal diluted fraction ratio leading to the maximal recovery ratio and energy storage performance. Higher hydraulic pressure difference is beneficial for recovery ratio and energy storage, while it hinders SEC and energy efficiency. After performance optimization, this system is capable to improve the maximal recovery ratio from 25%, 57% and 70% to 39%, 62% and 72% under the maximal bearable pressure difference of 4, 7 and 10 MPa, which proves the theoretical feasibility to achieve higher recovery ratio by the novel configuration. Moreover, maximal Gibbs free energy of 3.84 MJ can be stored with an overall energy efficiency of 8.42% while desalinating 1 m^3 seawater. As paring 0.5 m^3 brine solution that has the highest concentration of 2.18 M with 0.5 m^3 fresh river water, the salinity gradient energy is estimated by around 3.66 MJ. According to the overall analysis, this study offers a potential and sustainable method for synchronous water production and energy storage by solar energy powered high-recovery reverse osmosis system.

CRediT authorship contribution statement

Xiaotian Lai: Methodology, Visualization, Writing - original draft. **Rui Long:** Funding acquisition. **Zhichun Liu:** Funding acquisition. **Wei Liu:** Funding acquisition, Supervision.

Declaration of Competing Interest

The authors declare that they have no known competing financial interests or personal relationships that could have appeared to influence the work reported in this paper.

Acknowledgements

We acknowledge the support received from the National Natural Science Foundation of China (51736004, 51706076).

Appendix A

The derivation of discharged solution at the first stage and stored Gibbs free energy of self-diluted 2-stage reverse osmosis are stated in A.1 and A.2 respectively. And A.3 is the validation of reverse osmosis module.

A.1. Volume and concentration of brine solution at the first stage

The derivation of the discharged brine solution at the first stage is based on the conservation of dissolved ions in Eqs. (A-1) and (A-2), volume conservation of seawater in Eq. (A-3) and outlet concentration relationship in Eq. (A-4).

$$C_0(1-x) = C_{C,1}V_{C,1} \tag{A-1}$$

$$C_0 x = C_D V_D \tag{A-2}$$

$$V_{C,1} + V_D = 1 \tag{A-3}$$

$$2RT(C_{C,1} - C_D) = \Delta P \tag{A-4}$$

Substitute (A-3) and (A-4) into (A-2) to replace C_D and V_D with $C_{C,1}$ and $V_{C,1}$ in Eq. (A-5).

$$C_0 x = (C_{C,1} - \frac{\Delta P}{2RT})(1 - V_{C,1}) \tag{A-5}$$

Substituting (A-5) into (A-1), $C_{C,1}$ in Eq. (A-1) can be replaced by $V_{C,1}$ in the form of Eq. (A-6) to derive the quadratic equation of $V_{C,1}$ in Eq. (A-7).

$$C_{C,1} = C_0 + \frac{\Delta P}{2RT}(1 - V_{C,1}) \tag{A-6}$$

$$\frac{\Delta P}{2RT}V_{C,1}^2 - (C_0 + \frac{\Delta P}{2RT})V_{C,1} + C_0(1-x) = 0 \tag{A-7}$$

Eq. (A-7) indicates that two mathematical solutions of $V_{C,1}$ exist, which are derived as Eq. (A-8). For there is no discharged solution ($V_{C,1}$=0) as all the seawater is fed into the diluted channel ($x = 1$) at the first stage, the true solution of $V_{C,1}$ which has physical significance is Eq. (A-9).

$$V_{C,1} = (\frac{RTC_0}{\Delta P} + \frac{1}{2}) \pm \sqrt{(\frac{RTC_0}{\Delta P})^2 + (\frac{1}{2})^2 + \frac{RTC_0}{\Delta P}(2x-1)} \tag{A-8}$$

$$V_{C,1} = (\frac{RTC_0}{\Delta P} + \frac{1}{2}) - \sqrt{(\frac{RTC_0}{\Delta P})^2 + (\frac{1}{2})^2 + \frac{RTC_0}{\Delta P}(2x-1)} \tag{A-9}$$

According to Eq. (A-1), the concentration of the discharged brine solution at the first stage has Eq. (A-10).

$$C_{C,1} = \frac{C_0(1-x)}{V_{C,1}} = \frac{C_0(1-x)}{(\frac{RTC_0}{\Delta P} + \frac{1}{2}) - \sqrt{(\frac{RTC_0}{\Delta P})^2 + (\frac{1}{2})^2 + \frac{RTC_0}{\Delta P}(2x-1)}} \tag{A-10}$$

A.2. Gibbs free energy storage of Self-diluted 2-stage seawater reverse osmosis

The stored Gibbs free energy in the desalination process of source seawater exists between the generated fresh and brine solutions and has Eq. (A-11).

$$\Delta G_{\mathrm{RO}} = 2RT\left(V_{\mathrm{C}}\mathrm{C}_{\mathrm{C}} ln\frac{\mathrm{C}_{\mathrm{C}}}{\mathrm{C}_0} + \mathrm{V}_{\mathrm{F}}\mathrm{C}_{\mathrm{F}} ln\frac{\mathrm{C}_{\mathrm{F}}}{\mathrm{C}_0}\right) \tag{A-11}$$

In the self-diluted 2-stage SWRO, the volume and concentration of the brine and fresh solutions has following relationship with recovery ratio and initial concentration while desalinating 1 m^3 source seawater.

$$V_{\mathrm{F}} = \mathrm{Y} \tag{A-12}$$

$$V_{\mathrm{C}} = 1 - \mathrm{Y} \tag{A-13}$$

$$C_{\mathrm{F}} = 0 \tag{A-14}$$

$$C_{\mathrm{C}} = \frac{\mathrm{C}_0}{1 - \mathrm{Y}} \tag{A-15}$$

Substituting Eqs. (A-12)–(A-15) into Eq. (A-11), the stored Gibbs free energy has Eq. (A-16).

$$\Delta G_{\mathrm{RO}} = 2RT\left[C_0 ln\frac{1}{1-\mathrm{Y}} + \lim_{C\to 0}\left(\mathrm{YC} ln\frac{\mathrm{C}}{\mathrm{C}_0}\right)\right] \tag{A-16}$$

Adopting the L'Hospital's rule in Eq. (A-17), the second term in the square bracket in Eq. (A-16) equals to zero. Thus, the stored Gibbs free energy can be simplified as Eq. (A-18).

$$\lim_{C\to 0}\left(YCln\frac{C}{C_0}\right) = \lim_{C\to 0}\left(\frac{ln\frac{C}{C_0}}{\frac{1}{YC}}\right) = \lim_{C\to 0}\left(\frac{\frac{1}{C}}{-\frac{1}{YC^2}}\right) = \lim_{C\to 0}(-YC) = 0 \tag{A-17}$$

$$\Delta G_{\mathrm{RO}} = 2RTC_0 ln\frac{1}{1-\mathrm{Y}} \tag{A-18}$$

A.3. Validation of reverse osmosis module

In order to validate the derived analytical solution in this work, it is compared with a published mass transfer model from [41]. The main governing equations are stated below. At first, Eqs. (A-19)–(A-21) indicate the fundamental relationship of water transfer.

$$J_{\mathrm{w}} = A(\Delta P - \Delta\pi) = A[\Delta P - 2RT(C_{\mathrm{C}} - C_{\mathrm{D}})] \tag{A-19}$$

$$\frac{d\dot{V}_D}{dx} = J_{\mathrm{w}}W \tag{A-20}$$

$$\frac{d\dot{V}_C}{dx} = -J_{\mathrm{w}}W \tag{A-21}$$

Then, CP (concentration polarization) in the concentrated and diluted channels are considered as Eqs. (A-22) and (A-23). Thus, the transmembrane water flux is updated as Eq. (A-24).

$$C_{\mathrm{C,m}} = C_{\mathrm{C,b}} exp\left(\frac{J_{\mathrm{w}}}{k}\right) \tag{A-22}$$

$$C_{\mathrm{D,m}} = C_{\mathrm{D,b}} exp(-J_{\mathrm{w}}K) \tag{A-23}$$

$$J_{\mathrm{w}} = A\left\{\Delta P - 2RT\left[C_{\mathrm{C,b}} exp\left(\frac{J_{\mathrm{w}}}{k}\right) - C_{\mathrm{D,b}} exp(-J_{\mathrm{w}}K)\right]\right\} \tag{A-24}$$

Further considering RSP (reverse osmosis permeation) in Eq. (A-25) from the supporting information in [41], the molar flow rate of solutes varies in the form of Eq. (A-26) and (A-27).

$$J_{\mathrm{S}} = B(C_{\mathrm{C}} - C_{\mathrm{D}}) \tag{A-25}$$

$$\frac{d\left(\dot{V}_{\mathrm{D}}C_{\mathrm{D}}\right)}{dx} = J_{\mathrm{S}}W \tag{A-26}$$

$$\frac{d\left(\dot{V}_{\mathrm{C}}C_{\mathrm{C}}\right)}{dx} = -J_{\mathrm{S}}W \tag{A-27}$$

Compared with the mass transfer model stated above, this work attempts to evaluate the performance under sufficient membrane area condition.

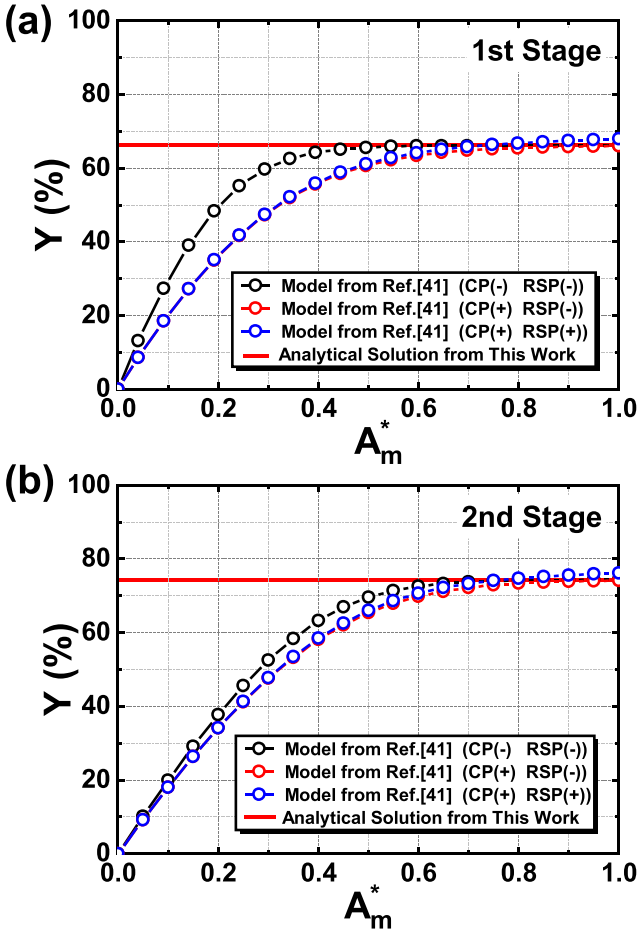

Fig. A-1. Validation of derived analytical solution.

Thus, we obtained the recovery ratio under zero membrane area ($A^*_m = 0$) to sufficient membrane area ($A^*_m = 1$) based on the mass transfer model in Fig. A-1 to compare with the recovery ratio obtained from this work. Relative parameter setting is referred from [41] as well.

In Fig. A-1, (a) and (b) depict the validation of the derived analytical solution in this work for the 1st and 2nd stage respectively. The black dot line is obtained from the fundamental water transfer relationship in which CP and RSP are neglected. It can be seen that with the increase of membrane area, recovery ratio goes up and reaches the value obtained by this work (red straight line). Then, CP is considered in the red dot line. It can be seen that CP increases the osmotic pressure difference as resistance. Thus, it needs more membrane area to achieve complete water permeation and reaches the red straight line. Finally, RSP is considered in the blue dot line, which is basically the same with the red dot line but a little bit higher. As membrane area is sufficient ($A^*_m = 1$), the relative error of recovery ratio at the 1st and 2nd stage is −2.62% and −2.40% respectively. This is because slight reverse salt permeation from the concentrated to diluted channel reduces the concentration difference. Thus, higher recovery ratio can be achieved under lower osmotic resistance. According to the comparison between the mass transfer model under ideal and realistic conditions with the analytical solution in this work at each stage, it can be seen that this work is capable to state a reliable performance evaluation of the novel RO configuration under sufficient membrane area condition.

References

[1] Scott CA, Pierce SA, Pasqualetti MJ, Jones AL, Montz BE, Hoover JH. Policy and institutional dimensions of the water–energy nexus. Energy Policy 2011;39:6622–30.
[2] Aboelmaaref MM, Zayed ME, Zhao J, Li W, Askalany AA, Salem Ahmed M, et al. Hybrid solar desalination systems driven by parabolic trough and parabolic dish CSP technologies: technology categorization, thermodynamic performance and economical assessment. Energy Convers Manage 2020;220:113103.
[3] Lv H, Wang Y, Wu L, Hu Y. Numerical simulation and optimization of the flash chamber for multi-stage flash seawater desalination. Desalination 2019;465:69–78.
[4] Liponi A, Wieland C, Baccioli A. Multi-effect distillation plants for small-scale seawater desalination: thermodynamic and economic improvement. Energy Convers Manage 2020;205:112337.
[5] Ruiz-Aguirre A, Andrés-Mañas JA, Fernández-Sevilla JM, Zaragoza G. Experimental characterization and optimization of multi-channel spiral wound air gap membrane distillation modules for seawater desalination. Sep Purif Technol 2018;205:212–22.
[6] Valladares Linares R, Li Z, Yangali-Quintanilla V, Ghaffour N, Amy G, Leiknes T, et al. Life cycle cost of a hybrid forward osmosis - low pressure reverse osmosis system for seawater desalination and wastewater recovery. Water Res 2016;88:225–34.
[7] Walker M, Seiler RL, Meinert M. Effectiveness of household reverse-osmosis systems in a Western U.S. region with high arsenic in groundwater. Sci Total Environ 2008;389:245–52.
[8] Kurihara M, Sasaki T, Nakatsuji K, Kimura M, Henmi M. Low pressure SWRO membrane for desalination in the Mega-ton Water System. Desalination 2015;368:135–9.
[9] Kim J, Park K, Hong S. Optimization of two-stage seawater reverse osmosis membrane processes with practical design aspects for improving energy efficiency. J Membr Sci 2020;601:117889.
[10] Delgado-Torres AM, García-Rodríguez L. Preliminary design of seawater and brackish water reverse osmosis desalination systems driven by low-temperature solar organic Rankine cycles (ORC). Energy Convers Manage 2010;51:2913–20.
[11] Kim J, Park K, Yang DR, Hong S. A comprehensive review of energy consumption of seawater reverse osmosis desalination plants. Appl Energy 2019;254:113652.

[12] Kim J, Hong S. A novel single-pass reverse osmosis configuration for high-purity water production and low energy consumption in seawater desalination. Desalination 2018;429:142–54.
[13] Seo J, Kim YM, Chae SH, Lim SJ, Park H, Kim JH. An optimization strategy for a forward osmosis-reverse osmosis hybrid process for wastewater reuse and seawater desalination: a modeling study. Desalination 2019;463:40–9.
[14] Baayyad I, Semlali Aouragh Hassani N, Bounahmidi T. Evaluation of the energy consumption of industrial hybrid seawater desalination process combining freezing system and reverse osmosis. Desalin Water Treat 2014;56:2593–601.
[15] Kim S, Rahardianto A, Walker JS, Wolfe T, Coleman K, Cohen Y. Upgrading polyamide TFC BWRO and SWRO membranes to higher SWRO membrane performance via surface nano-structuring with tethered poly(acrylic acid). J Membr Sci 2020;597:117736.
[16] Su X, Li W, Palazzolo A, Ahmed S. Concentration polarization and permeate flux variation in a vibration enhanced reverse osmosis membrane module. Desalination 2018;433:75–88.
[17] Yan Z, Yang H, Qu F, Yu H, Liang H, Li G, et al. Reverse osmosis brine treatment using direct contact membrane distillation: effects of feed temperature and velocity. Desalination 2017;423:149–56.
[18] Cameron IB, Clemente RB. SWRO with ERI's PX pressure exchanger device — a global survey. Desalination 2008;221:136–42.
[19] Touati K, Tadeo F, Elfil H. Osmotic energy recovery from Reverse Osmosis using two-stage Pressure Retarded Osmosis. Energy. 2017;132:213–24.
[20] Giacalone F, Papapetrou M, Kosmadakis G, Tamburini A, Micale G, Cipollina A. Application of reverse electrodialysis to site-specific types of saline solutions: a techno-economic assessment. Energy 2019;181:532–47.
[21] Sivaram PM, Mande AB, Premalatha M, Arunagiri A. Investigation on a building-integrated passive solar energy technology for air ventilation, clean water and power. Energy Convers Manage 2020;211:112739.
[22] Eveloy V, Rodgers P, Qiu L. Integration of an atmospheric solid oxide fuel cell – gas turbine system with reverse osmosis for distributed seawater desalination in a process facility. Energy Convers Manage 2016;126:944–59.
[23] He W, Wang Y, Sharif A, Shaheed MH. Thermodynamic analysis of a stand-alone reverse osmosis desalination system powered by pressure retarded osmosis. Desalination 2014;352:27–37.
[24] Peñate B, Castellano F, Bello A, García-Rodríguez L. Assessment of a stand-alone gradual capacity reverse osmosis desalination plant to adapt to wind power availability: a case study. Energy. 2011;36:4372–84.
[25] Delgado-Torres AM, García-Rodríguez L, del Moral MJ. Preliminary assessment of innovative seawater reverse osmosis (SWRO) desalination powered by a hybrid solar photovoltaic (PV) – tidal range energy system. Desalination 2020;477:114247.
[26] Bayrak F, Oztop HF, Selimefendigil F. Experimental study for the application of different cooling techniques in photovoltaic (PV) panels. Energy Convers Manage 2020;212:112789.
[27] Dong Q, Liao T, Yang Z, Chen X, Chen J. Performance characteristics and parametric choices of a solar thermophotovoltaic cell at the maximum efficiency. Energy Convers Manage 2017;136:44–9.
[28] Biencinto M, González L, Valenzuela L, Zarza E. A new concept of solar thermal power plants with large-aperture parabolic-trough collectors and sCO2 as working fluid. Energy Convers Manage 2019;199:112030.
[29] Shalaby SM. Reverse osmosis desalination powered by photovoltaic and solar Rankine cycle power systems: a review. Renew Sustain Energy Rev 2017;73:789–97.
[30] Abbasi HR, Pourrahmani H, Yavarinasab A, Emadi MA, Hoorfar M. Exergoeconomic optimization of a solar driven system with reverse osmosis desalination unit and phase change material thermal energy storages. Energy Convers Manage 2019;199:112042.
[31] Vyas H, Suthar K, Chauhan M, Jani R, Bapat P, Patel P, et al. Modus operandi for maximizing energy efficiency and increasing permeate flux of community scale solar powered reverse osmosis systems. Energy Convers Manage 2015;103:94–103.
[32] Hafez AZ, Soliman A, El-Metwally KA, Ismail IM. Design analysis factors and specifications of solar dish technologies for different systems and applications. Renew Sustain Energy Rev 2017;67:1019–36.
[33] He W, Wang J. Feasibility study of energy storage by concentrating/desalinating water: concentrated water energy storage. Appl Energy 2017;185:872–84.
[34] Lai X, Yu M, Long R, Liu Z, Liu W. Dynamic performance analysis and optimization of dish solar Stirling engine based on a modified theoretical model. Energy. 2019;183:573–83.
[35] Rovense F, Reyes-Belmonte MA, González-Aguilar J, Amelio M, Bova S, Romero M. Flexible electricity dispatch for CSP plant using un-fired closed air Brayton cycle with particles based thermal energy storage system. Energy 2019;173:971–84.
[36] Kovač M, Stegnar G, Al-Mansour F, Merše S, Pečjak A. Assessing solar potential and battery instalment for self-sufficient buildings with simplified model. Energy 2019;173:1182–95.
[37] Nagy E, Dudás J, Hegedüs I. Improvement of the energy generation by pressure retarded osmosis. Energy 2016;116:1323–33.
[38] Kim YC, Elimelech M. Potential of osmotic power generation by pressure retarded osmosis using seawater as feed solution: analysis and experiments. J Membr Sci 2013;429:330–7.
[39] Kurihara M, Yamamura H, Nakanishi T, Jinno S. Operation and reliability of very high-recovery seawater desalination technologies by brine conversion two-stage RO desalination system. Desalination 2001;138:191–9.
[40] Kurihara M, Yamamura H, Nakanishi T. High recovery/high pressure membranes for brine conversion SWRO process development and its performance data. Desalination 1999;125.
[41] Bartholomew TV, Mey L, Arena JT, Siefert NS, Mauter MS. Osmotically assisted reverse osmosis for high salinity brine treatment. Desalination 2017;421:3–11.
[42] Chen X, Yip NY. Unlocking high-salinity desalination with cascading osmotically mediated reverse osmosis: energy and operating pressure analysis. Environ Sci Technol 2018;52:2242–50.
[43] Bouma AT, Lienhard JH. Split-feed counterflow reverse osmosis for brine concentration. Desalination 2018;445:280–91.
[44] Banan Sadeghian R, Pantchenko O, Tate D, Shakouri A. Miniaturized concentration cells for small-scale energy harvesting based on reverse electrodialysis. Appl Phys Lett 2011;99:173702.
[45] Lai X, Yu M, Long R, Liu Z, Liu W. Clean and stable utilization of solar energy by integrating dish solar Stirling engine and salinity gradient technology. Energy 2019;182:802–13.